Simultaneous Deterministic Control of Distant Qubits in Two Semiconductor Quantum Dots

A. Gamouras,[†] R. Mathew,[†] S. Freisem,[‡] D. G. Deppe,[‡] and K. C. Hall[*,†]

Department of Physics and Atmospheric Science, Dalhousie University, Halifax, Nova Scotia B3H4R2, Canada, and The College of Optics and Photonics, University of Central Florida, Orlando, Florida 32816-2700, USA

E-mail: kimberley.hall@dal.ca

Phone: (902) 494 7109. Fax: (902) 494 5191

Supporting Information

Materials and Methods

Experimental Techniques

The optical source used in this work is a wavelength tunable 76 MHz optical parametric oscillator laser system producing optical pulses around 1.2 μm. The self-assembled InAs/GaAs quantum dot wafer was mounted on an attocube nanopositioning stage inside a helium flow microscopy cryostat at 10 K, as shown in Fig. S1. A high numerical aperture microscope objective (NA 0.7, 100$\times$) designed for infrared wavelengths was used for both laser excitation and collection of the emitted

[*]To whom correspondence should be addressed
[†]Department of Physics and Atmospheric Science, Dalhousie University, Halifax, Nova Scotia B3H4R2, Canada
[‡]The College of Optics and Photonics, University of Central Florida, Orlando, Florida 32816-2700, USA

photoluminescence. The photoluminescence spectrum was detected using a 0.75 m monochromator with 30 μeV spectral resolution and a liquid nitrogen-cooled InGaAs array detector.

An ideal *unshaped* control laser pulse has a constant phase, leading to the shortest possible temporal duration considering its frequency bandwidth. Such a pulse is referred to as a transform-limited (TL) pulse. The typical output from ultrafast oscillator laser systems is generally not an ideal TL pulse, but can exhibit significant linear and higher order phase structure (*i.e.* the pulse phase has an unintended frequency dependence, called *chirp*). In addition, the optical pulse can accumulate phase structure by propagating through various optical components in the experimental apparatus. The associated unintended phase structure must be characterized and compensated for prior to application of the optimum shaping mask. This process is called dispersion compensation, and is carried out in this work using multiphoton intrapulse interference phase scan (MIIPS).[2] The pulse shaping system used in these experiments consists of an infrared 4f pulse shaper incorporating a computer controlled dual mask 128 pixel spatial light modulator (SLM). Feedback to the pulse shaping system for dispersion compensation using MIIPS was provided by the second harmonic spectrum, in which a BBO nonlinear crystal was placed at an equivalent focus to the sample position. Application of the dispersion compensation phase mask determined using MIIPS resulted in an optimized unshaped pulse with a duration of 130 fs, within 1 % of the TL value (*i.e.* $\tau/\tau_{\mathrm{TL}} \leq 1.01$, where τ = 130 fs and τ_{TL} is the ideal pulse duration dictated by the measured pulse bandwidth). This dispersion compensation phase mask was added to the calculated optimum phase mask for the phase control experiments. Figure S2 shows calculated MIIPS traces for the TL as well as the shaped optical pulses. The equally spaced parallel lines in Fig. S2a are characteristic of a TL optical pulse, while the cross-hatched pattern in Fig. S2b is a signature of the cosine phase function used here. The measured interferometric autocorrelation for the dispersion compensated pulse is shown in Fig. S2c, together with the corresponding calculated autocorrelation in Fig. S2d. Calculated MIIPS and autocorrelation plots for both TL and shaped pulses are in agreement with the experimentally measured traces shown in Fig. S2 and Fig. 2 in the main text.

The Gaussian beam spot size of the focused excitation laser at the sample, required for cal-

culation of the electric dipole moments of the selected quantum dots, was determined using a knife-edge type measurement. The focused laser beam was reflected off a laterally translating metallic step edge on the masked quantum dot sample within the microscopy cryostat. The resulting change in reflectivity was measured using an InGaAs photodiode. The collected reflectivity data was differentiated and fit to a Gaussian function to extract the laser spot size.

Sample

The InAs/GaAs quantum dot structure was grown by molecular beam epitaxy under conditions optimized for a sparse quantum dot ensemble with the ground state optical transition of the quantum dots near 1.3 μm. The single quantum dot layer was deposited on top of 200 nm of GaAs under indium-rich conditions. The quantum dots were overgrown with $In_{0.2}Ga_{0.8}As$ at a low growth temperature to reduce intermixing, followed by 65 nm of GaAs. AlGaAs carrier blocking layers were deposited above and below the GaAs layers. The photoluminescence for this structure is shown in Fig. S3. From corresponding photoluminescence excitation experiments, we determined that the peaks in Fig. S3b at 0.965 eV (1285 nm) and 1.017 eV (1220 nm) are due to ground state emission from two distinct subsets of quantum dots within the ensemble. The separation between the ground state and excited state transitions in these subsets are 95 meV and 75 meV averaged over the ensemble, respectively. As a result, the small peak at 1.083 eV (1145 nm) in Fig. S3b is attributed to the excited state transition in the higher-energy subset of quantum dots. The lower-energy quantum dot subset has an estimated areal density of 6×10^9 cm^{-2}, an average quantum dot height of 9 nm and a lateral size of 20 nm from cross-sectional transmission electron microscopy and atomic force microscopy on similar structures. To facilitate spectral isolation of individual quantum dots, a metallic mask containing an array of apertures of varying sizes (0.1 μm to 1.0 μm) was deposited onto the sample surface. Microphotoluminescence measurements, using 830 nm continuous wave laser excitation, show single quantum dot peaks in both subsets of the ensemble (Fig. S3). The experiments reported here were carried out on quantum dots within a 0.4 μm aperture in the lower-energy subset. The power-dependence of the s-shell μPL for QD1 (QD2)

is shown in Fig. S3**d** (Fig. S3**e**). The saturation of the s-shell emission for high pump powers has been observed in similar QDs.[3]

Description of Model

The theoretical model treats QD1 and QD2 as independent two-level systems, each consisting of a vacuum state $|g\rangle$ and p-shell exciton state $|e\rangle$ with their respective transition energies $\hbar\omega_{eg}$. The quantum states are manipulated using the electric field of a laser pulse given by,

$$\vec{E}(t) = \frac{1}{2}\hat{\varepsilon}E_0(t)[\exp(-i\omega_0 t - i\phi(t)) + \exp(i\omega_0 t + i\phi(t))], \tag{1}$$

where ω_0 is the center frequency of the laser pulse, $\phi(t)$ is the temporal phase, and $E_0(t)$ is the electric field envelope. In the calculation, the envelope is taken to be in the form:

$$E_0(t) = |E_0|\text{sech}(1.76t/\tau), \tag{2}$$

where τ is the pulse width. For a transform-limited pulse, $\phi(t) = \phi_0$ is constant. The interaction of the electric field with each quantum dot is calculated using the Liouville equation for the density matrix

$$\dot{\rho} = \frac{i}{\hbar}[\rho, H_0 + H_{\text{int}}], \tag{3}$$

where H_0 is the unperturbed Hamiltonian and $H_{\text{int}} = -\vec{\mu}\cdot\vec{E}(t)$ is the interaction Hamiltonian with dipole moment operator $\vec{\mu}$. The resulting optical Bloch equations in the rotating wave approximation, with change of variables $\rho_{ij} \rightarrow \tilde{\rho}_{ij}$ to remove fast variations in the coherences, are given by

$$\dot{\tilde{\rho}}_{ee} = (-i/2)\left[\Omega_R\tilde{\rho}_{ge} - \tilde{\rho}_{eg}\Omega_R^*\right] - \Gamma_{ee}\tilde{\rho}_{ee}, \tag{4a}$$

$$\dot{\tilde{\rho}}_{eg} = (-i/2)\left[2\Delta\tilde{\rho}_{eg} - \Omega_R(2\tilde{\rho}_{ee} - 1)\right] - \Gamma_{eg}\tilde{\rho}_{eg}, \tag{4b}$$

where $\Omega_R = -\mu_{eg}E_0(t)/\hbar$ is the complex Rabi frequency, $\Delta \equiv \omega_{eg} - \omega$ is the laser detuning, ρ_{ee} is the population in state $|e\rangle$, and ρ_{eg} is the coherence between states $|e\rangle$ and $|g\rangle$. Γ_{ee} and Γ_{eg} are the constant population decay rate and constant dephasing rate, respectively. The density matrix for the combined system is the direct product of the density matrices for the two quantum dots ($\rho = \rho_1 \otimes \rho_2$) and the fidelity of the operation is defined as

$$F = \mathrm{Tr}[\rho_{\mathrm{ph}}\rho_{\mathrm{id}}], \tag{5}$$

where ρ_{ph} is the physical density matrix for a given laser pulse and ρ_{id} is the ideal density matrix for the quantum gate.

We engineer the quantum state evolution of QD1 and QD2 by manipulating $E(t)$, and hence H_{int}, using a 4f pulse shaper, which provides independent control over the frequency-dependent amplitude and phase of the pulse. The effect of the SLM in the pulse shaper may be modeled as a linear filter with a frequency response $M(\omega)$ given by

$$M(\omega) = A_M(\omega)\exp\left[i\Phi_M(\omega)\right], \tag{6}$$

where $A_M(\omega)$ and $\Phi_M(\omega)$ are user-defined amplitude and phase functions. The Fourier transform of the laser pulse after the shaper, $\tilde{E}_{\mathrm{out}}$, is related to the input pulse, $\tilde{E}_{\mathrm{in}}$, by

$$\tilde{E}_{\mathrm{out}}(\omega) = \tilde{E}_{\mathrm{in}}(\omega)M(\omega). \tag{7}$$

The use of MIIPS for dispersion compensation allows us to assume a transform-limited input pulse $\tilde{E}_{\mathrm{in}}(\omega)$. For the purposes of this study we set $A_M(\omega) = 1$ and use phase-only control, which serves to conserve pulse power. The functional form of $\Phi_M(\omega)$ was chosen to be

$$\Phi_M(\omega) = \alpha\cos[\gamma(\omega - \omega_0) - \varphi], \tag{8}$$

where α is the amplitude, γ is the spectral frequency, and φ is the phase shift. The fidelity $F = f(\alpha, \gamma, \varphi, \Theta)$ of the operation is optimized as a function of α, γ, φ and the pulse area ($\Theta = (\vec{\mu} \cdot \hat{\varepsilon}/\hbar) \int_{-\infty}^{+\infty} E_0(t)\, dt$).

During optimization, the parameters are subject to the following constraints

$$0 \leq \alpha \leq \pi, \tag{9a}$$

$$0 \leq \gamma \leq 315\,\text{fs}, \tag{9b}$$

$$-\pi \leq \varphi \leq \pi, \tag{9c}$$

$$\pi/2 \leq \Theta \leq 5\pi/2. \tag{9d}$$

The constraints on α and γ serve to restrict the gradient in the phase to approximately $\pi/10$ radians per pixel, a conservative restriction for the 128-pixel SLM used in this work, while the constraint on Θ limits the optimized pulse shapes to relatively low pulse areas.

To optimize the fidelity of the quantum gate, we choose a mask function defined by a vector $q_i = \{\alpha_i, \gamma_i, \varphi_i, \Theta_i\}$ within the parameter space defined by equation 9, apply the mask to a TL pulse (with the experimentally measured pulse width of 130 fs), and calculate the electric field which dictates the time dependence of the interaction Hamiltonian. We then integrate the Bloch equations (equation 4) to determine the state dynamics and the fidelity F_i (equation 5). The vector q_i is driven towards a local optimum in fidelity F_{opt} with associated vector $q_{opt} = \{\alpha_{opt}, \gamma_{opt}, \varphi_{opt}, \Theta_{opt}\}$ using the constrained optimization by linear approximations (COBYLA) algorithm.[4] We find that repeating this procedure with 500 initial vectors q_i, selected using a quasi-random Sobol' sequence,[5] provides sufficient coverage of the parameter space to find a q_{opt} vector with high fidelity ($F > 0.95$).

Shown in Fig. S4 is a comparison of the pulse characteristics and quantum state dynamics for a TL pulse Fig. S4(d, e, f) and a shaped pulse Fig. S4(a, b, c) corresponding to the highest gate fidelity found by the optimization algorithm. (The quantum gate is the same as that described in the main text, i.e. a π rotation for QD2 and 2π rotation for QD1.) The shaped pulse is defined by the vector $q = \{0.9960\pi, 307.1\,\text{fs}, -0.5751\pi, 2.042\pi\}$. The first column of panels in Fig. S4

shows the spectral amplitude and phase, and the second column displays the electric field intensity as a function of time for both pulses. The third column of panels presents the resulting occupation dynamics of the p-shell exciton state $|e\rangle$ as a function of time for QD2 and QD1. The pulse area of the TL pulse is chosen to match that of the shaped pulse (i.e. $\Theta = 2.042\pi$). The shaped pulse executes the gate with a fidelity of 0.968 compared to 0.294 for the TL pulse.

Experimental Limitations on Gate Fidelity

Practical limits on the performance of the quantum gate considered in this work were assessed by calculating the gate fidelity including sources of experimental error. This allows us to gauge the sensitivity of quantum gates more generally for the physical implementation of exciton qubits in self-assembled quantum dots. The laser source exhibits fluctuations in pulse to pulse intensity ($\pm$0.5 %) and in centre pulse wavelength ($\pm$0.2 nm). The associated reductions in fidelity are 0.005 and 0.01, respectively. The wavelength instability arises from active feedback in the optical parametric oscillator laser source used in this work. The accuracy of the applied pulse shape is limited by the quality of dispersion compensation, which is indicated by the ratio τ/τ_{TL}, which is typically 1.002 in our experiments. Taking a more conservative value of τ/τ_{TL} = 1.01 and including the associated residual phase distortions in the theoretical calculations by adding a corresponding amount of linear chirp, we obtain ΔF = 0.005. For experimental uncertainties in the quantum dot electronic structure parameters (p-shell transition energy, dipole moment), the reduction in fidelity was largest when including deviations from the measured values for QD1, reflecting the robustness of adiabatic passage on QD2. For QD1, the $\pm$0.25 meV uncertainty in the transition energy (from photoluminescence excitation measurements) and $\pm$5% for the dipole moment (from Rabi oscillations), each result in a reduction in fidelity of 0.01. For schemes involving optical control of the s-shell transition (using *e.g.* quantum state readout via a resonance fluorescence configuration[6] or detection of the nonlinear optical response[7]), the uncertainty in the transition energy would be smaller, limited only by the $\sim$ 50-100 μeV linewidth of the s-shell due to spectral wandering.[8] The

relevant experimental error in the dipole moment for design of the gate pulse is the measurement error for the laser power required for a Rabi oscillation. Decay and decoherence are incorporated into the calculations within the relaxation time approximation.[9] For the s-shell transition, four-wave mixing experiments on similar InAs QDs indicated a radiatively-limited decoherence time of 1 ns at low temperature.[10] For the p-shell transition, T_2 is several tens of picoseconds, limited by energy relaxation to the s-shell.[11] Due to the short time scale of the control pulse relative to these relaxation times, the influence of decoherence on gate fidelity is small. For quantum computing applications, optical control of the s-shell is preferred due to the much longer lifetime of the qubit *after the control pulse is over*. The reduction in fidelity due to decoherence and relaxation using typical values of T_1 and T_2 for the s-shell in these quantum dots[8,10] is 0.005, similar to the calculated gate errors associated with other uncertainties, as described above. These small errors are promising for the prospect of realising practical quantum computing hardware based on self-assembled quantum dots.

References

(1)

(2) Lozovoy, V. V.; Pastirk, I.; Dantus, M. *Opt. Lett.* **2004**, *29*, 775–777.

(3) Kamada, H.; Ando, H.; Temmyo, J.; Tamamura, T. *Phys. Rev. B* **1998**, *58*, 16243–16251.

(4) Powell, M. A DIRECT SEARCH OPTIMIZATION METHOD THAT MODELS THE OBJECTIVE AND CONSTRAINT FUNCTIONS BY LINEAR INTERPOLATION. *Advances in optimization and numerical analysis: proceedings of the Sixth Workshop on Optimization and Numerical Analysis, Oaxaca, Mexico*, 1994; p 51.

(5) Sobol, I. M. *Computational mathematics and mathematical physics* **1967**, *7*, 86+.

(6) Muller, A.; Flagg, E. B.; Bianucci, P.; Wang, X. Y.; Deppe, D. G.; Ma, W.; Zhang, J.; Salamo, G. J.; Xiao, M.; Shih, C. K. *Phys. Rev. Lett.* **2007**, *99*, 187402.

(7) Kim, E. D.; Truex, K.; Wu, Y.; Amo, A.; Xu, X.; Steel, D. G.; Bracker, A. S.; Gammon, D.; Sham, L. J. *Applied Physics Letters* **2010**, *97*, 113110.

(8) Borri, P.; Langbein, W.; Schneider, S.; Woggon, U.; Sellin, R. L.; Ouyang, D.; Bimberg, D. *Phys. Rev. Lett.* **2001**, *87*, 157401.

(9) Mathew, R.; Pryor, C. E.; Flatté, M. E.; Hall, K. C. *Phys. Rev. B* **2011**, *84*, 205322.

(10) Langbein, W.; Borri, P.; Woggon, U.; Stavarache, V.; Reuter, D.; Wieck, A. D. *Phys. Rev. B* **2004**, *70*, 033301.

(11) Htoon, H.; Kulik, D.; Baklenov, O.; Holmes, A. L.; Takagahara, T.; Shih, C. K. *Phys. Rev. B* **2001**, *63*, 241303.

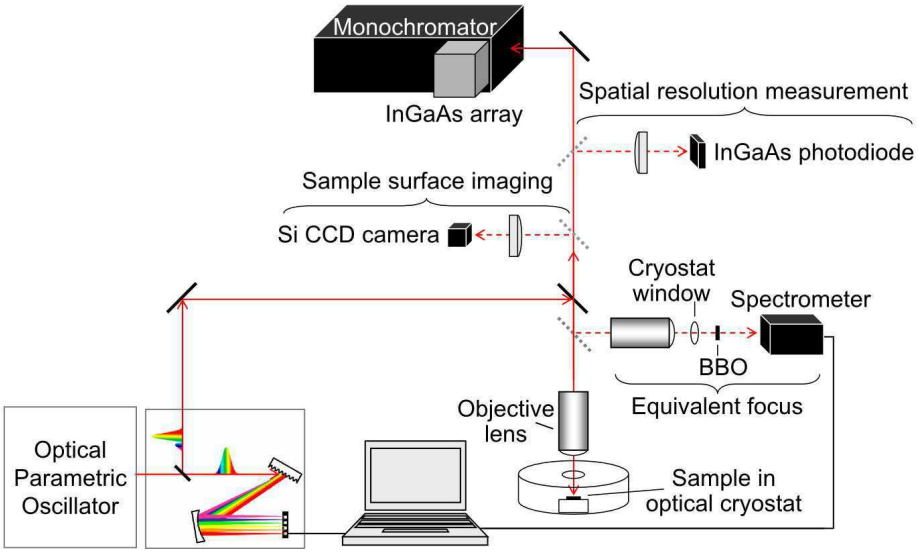

Figure S1: Diagram of quantum control apparatus showing alignment configurations for laser spot size measurement and imaging of quantum dot sample surface.

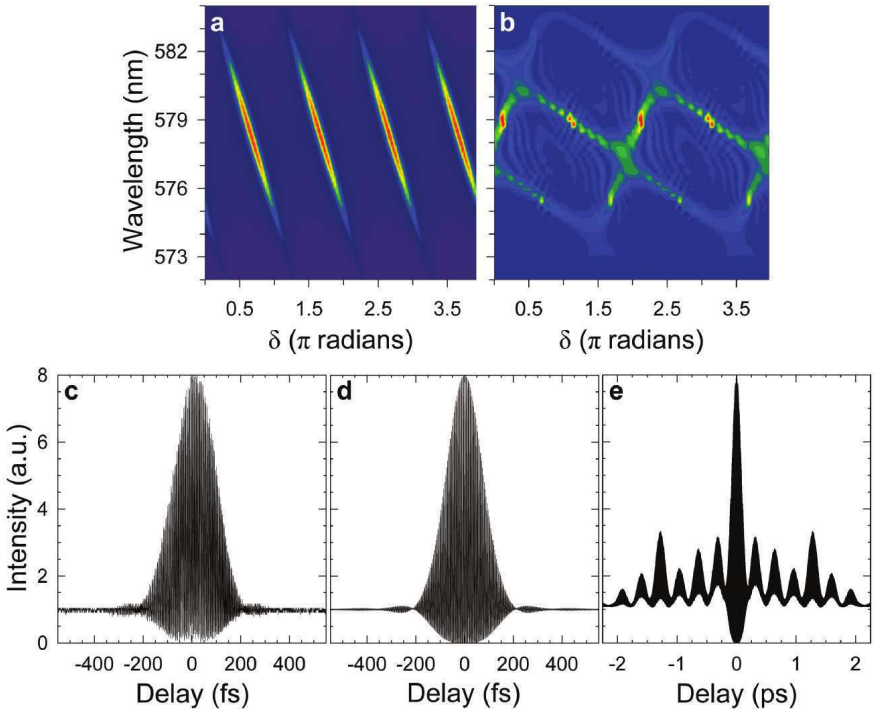

Figure S2: Calculated MIIPS traces of (**a**) the transform-limited pulse and (**b**) the phase shaped control pulse. **c**, Measured interferometric autocorrelation of the dispersion-compensated pulse. Calculated autocorrelation traces of (**d**) the transform-limited pulse and (**e**) the phase shaped control pulse.

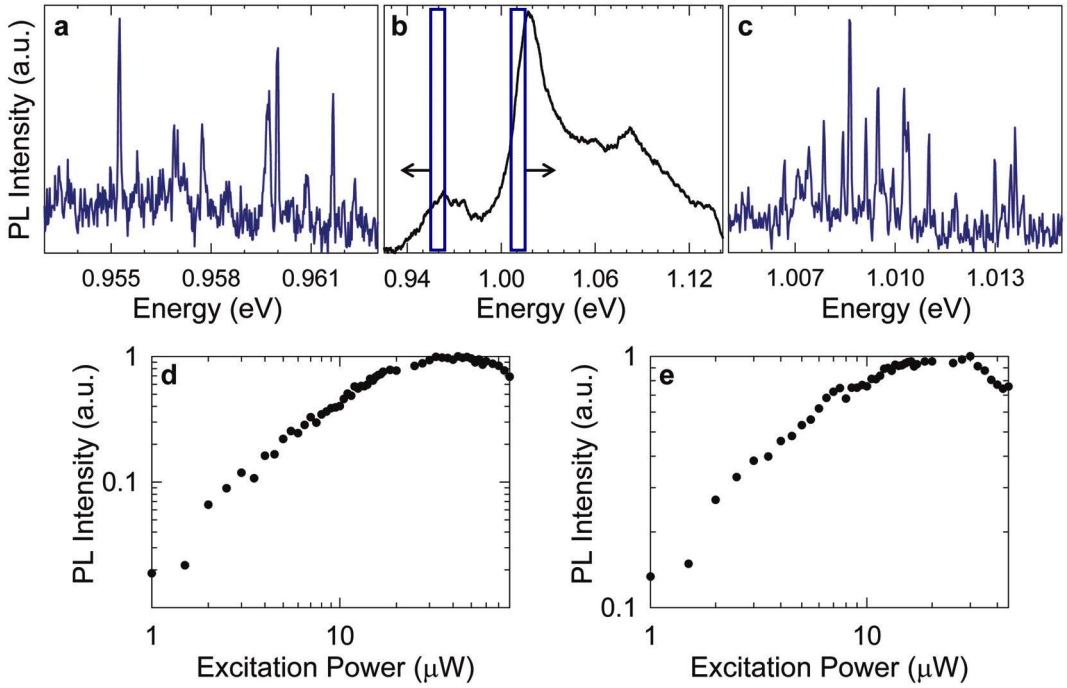

Figure S3: Photoluminescence spectra from the InAs/GaAs QD structure at 10 K. **a**, Microphotoluminescence from the lower-energy QD subset. **b**, Ensemble PL from the unmasked QD structure. The rectangles indicate the energy ranges of microphotoluminescence in **a** and **c**. **c**, Microphotoluminescence from the higher-energy QD subset. **d**(**e**): Power dependence of the s-shell emission observed in μPL for QD1 (QD2).

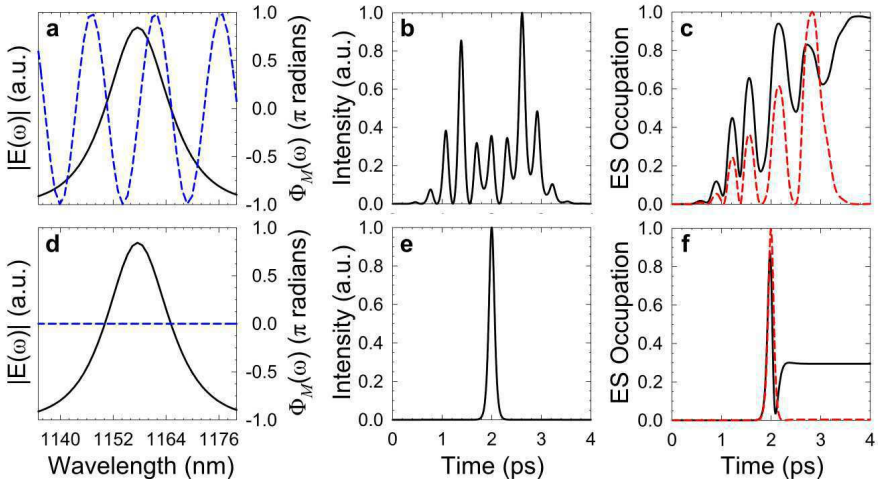

Figure S4: Pulse characteristics and population dynamics for a shaped pulse (**a, b, c**) and a transform-limited pulse (**d, e, f**). **a** and **d** show the amplitude (solid black curve) and phase (dashed blue curve). **b** and **e** show the temporal electric field intensity. **c** and **f** show the population dynamics of the p-shell exciton state (ES) for QD1 (red dashed curve) and QD2 (black solid curve).